THE JOURNAL OF BIOLOGICAL CHEMISTRY
Vol. 277, No. 32, Issue of August 9, pp. 29086–29093, 2002

Printed in U.S.A.

Crystal Structure of Human Group X Secreted Phospholipase A_2

ELECTROSTATICALLY NEUTRAL INTERFACIAL BINDING SURFACE TARGETS ZWITTERIONIC MEMBRANES*

Received for publication, March 15, 2002, and in revised form, May 20, 2002
Published, JBC Papers in Press, May 25, 2002, DOI 10.1074/jbc.M202531200

Ying H. Pan‡, Bao-Zhu Yu‡, Alan G. Singer§, Farideh Ghomashchi§, Gérard Lambeau¶, Michael H. Gelb§, Mahendra K. Jain‡, and Brian J. Bahnson‡‖

From the ‡Department of Chemistry and Biochemistry, University of Delaware, Newark, Delaware 19716, the §Departments of Chemistry and Biochemistry, University of Washington, Seattle, Washington 98195, and the ¶Institut de Pharmacologie Moléculaire et Cellulaire, CNRS-UPR 411, 660 route des Lucioles, Sophia Antipolis 06560 Valbonne, France

The crystal structure of human group X (hGX) secreted phospholipase A_2 ($sPLA_2$) has been solved to a resolution of 1.97 Å. As expected the protein fold is similar to previously reported $sPLA_2$ structures. The active site architecture, including the positions of the catalytic residues and the first and second shell water around the Ca^{2+} cofactor, are highly conserved and remarkably similar to the group IB and group IIA enzymes. Differences are seen in the structures following the (1–12)-N-terminal helix and at the C terminus. These regions are proposed to interact with the substrate membrane surface. The opening to the active site slot is considerably larger in hGX than in human group IIA $sPLA_2$. Furthermore, the electrostatic surface potential of the hGX interfacial-binding surface does not resemble that of the human group IIA $sPLA_2$; the former is highly neutral, whereas the latter is highly cationic. The cationic residues on this face of group IB and IIA enzymes have been implicated in membrane binding and in k^*_{cat} allostery. In contrast, hGX does not show activation by the anionic charge at the lipid interface when acting on phospholipid vesicles or short-chain phospholipid micelles. Together, the crystal structure and kinetic results of hGX supports the conclusion that it is as active on zwitterionic as on anionic interfaces, and thus it is predicted to target the zwitterionic membrane surfaces of mammalian cells.

Recent molecular cloning studies have shown that mammals contain a large number of secreted phospholipases A_2 ($sPLA_2$),[1] 9 gene products in humans and 10 in mice (1, 2). These 14–18-kDa disulfide-rich proteins require Ca^{2+} as a catalytic cofactor for the hydrolysis of the *sn*-2 ester of glycerophospholipids at the interface. For the past 4 decades the 14-kDa pancreatic group IB $sPLA_2$ has been a paradigm for interfacial enzymes that exhibit processive turnover at the substrate interface (3–5). The other $sPLA_2$ family members are of interest because they often act in concert with intracellular 87-kDa phospholipase A_2 to liberate arachidonic acid from cellular phospholipids as the substrate for the eicosanoid pathways (6–8). We are now faced with the challenge of understanding the physiological functions of the full set of mammalian $sPLA_2$s. The fact that each of these enzymes has distinct expression profiles and tissue distributions argues that they do not have redundant functions, although such functions remain to be established. Also, the tissue distribution of a particular human $sPLA_2$ is often distinct from that of its mouse ortholog (1). Thus, one cannot always infer the function of a human $sPLA_2$ from genetic studies with $sPLA_2$-deficient mice. It appears that, coupled with biochemical characterization of their function, highly selective inhibitors for each $sPLA_2$ gene product could facilitate the search for their specific physiological functions.

A portion of the gene that codes for the human group X $sPLA_2$ (hGX) was identified in GenBank™, and the full-length sequence was obtained from a fetal lung cDNA library (9). This $sPLA_2$ contains a disulfide pattern that is a combination of some of the unique disulfides found in group I and II $sPLA_2$s. Furthermore, hGX lacks the loops that are characteristic of the pancreatic and elapid snake enzymes, and was therefore given the unique name group X (9). The mRNA for hGX was found in spleen, thymus, peripheral blood leukocytes, and to a lesser extent in pancreas, lung, and colon cells (9). Unlike the group IB and IIA $sPLA_2$s that display significant preference for vesicles of anionic phospholipids (10), hGX is able to hydrolyze phosphatidylcholine-rich vesicles at a rate comparable with its action on anionic phospholipid vesicles (11). As a result, hGX is able to potently release arachidonic acid when added exogenously to the phosphatidylcholine-rich extracellular face of the plasma membrane of a variety of mammalian cells (11–13). Based on this specificity profile, hGX has been implicated to play a critical role in the arachidonic acid-mediated cyclooxygenase-2 pathway during colon carcinogenesis (14). There are dramatically different affinities of the various $sPLA_2$s for membrane surfaces containing different phospholipids. This is likely to be controlled by the amino acid differences that lie on their interfacial binding surfaces (i-face) rather than the substrate affinity controlled by the active site residues. The i-face is the nearly planar surface of $sPLA_2$s that surrounds the opening to the active site slot. The later is a ~15-Å deep pocket

* This work was supported in part by Grants GM-29703 (to M. K. J. and B. J. B.) and HL-36235 (to M. H. G.) from the National Institutes of Health, the CNRS, the Association pour la Recherche sur le Cancer (ARC), the Fonds de Recherche Hoechst Marion Roussel, and the Agence Nationale de Recherches contre le Sida (ANRS).

The atomic coordinates and structure factors (code 1LE6 and 1LE7) have been deposited in the Protein Data Bank, Research Collaboratory for Structural Bioinformatics, Rutgers University, New Brunswick, NJ (http://www.rcsb.org/).

‖ To whom correspondence should be addressed. Tel.: 302-831-0786; Fax: 302-831-6335; E-mail: bahnson@udel.edu.

[1] The abbreviations used are: $sPLA_2$, secreted phospholipase A_2; B-factor, temperature factor; CMC, critical micelle concentration; DC_nPC, 1,2-diacylglycero-*sn*-3-phosphocholine with *n* carbons in each acyl chain; DC_nPM, 1,2-diacylglycero-*sn*-3-phosphomethanol with *n* carbons in each acyl chain; DC_6PC-ether, 1,2-dihexylglycero-*sn*-3-phosphocholine; hGIIA, human group IIA $sPLA_2$; hGX, human group X $sPLA_2$; i-face; interface binding surface of enzyme; MJ33, 1-hexadecyl-3-(trifluoroethyl)-*sn*-glycero-2-phosphomethanol; MPD, 2-methyl-2,4-pentanediol; pGIB, porcine group IB $sPLA_2$; R_{free}, free *R*-factor; $R_{working}$, working *R*-factor.

of sPLA$_2$s where a single phospholipid molecule must enter to reach the catalytic residues necessary for ester bond hydrolysis (5, 15–17).

The goal of the present study was to obtain structural information of the hGX enzyme to provide clues into its substrate and interface specificity, mode of interfacial activation, and most importantly its physiological function. Here we report the 1.97-Å crystal structure of a ligand-free form of hGX as a prelude to understanding the i-face residues that allow its relatively high affinity for phosphatidylcholine-rich membranes. We also gain insight into structure-based design of inhibitors that are selective for this sPLA$_2$. Attempts were made to obtain the structure with and without the active- site inhibitor 1-hexadecyl-3-(trifluoroethyl)-*sn*-glycero-2-phosphomethanol (MJ33) (18). Two crystal forms were obtained that led to independent structures of hGX, both without bound inhibitor.

EXPERIMENTAL PROCEDURES

Expression and Purification of hGX—The hGX was purified by a new procedure that gives improved yield compared with our original procedure (11). Sulfonated fusion protein was dissolved to 10 mg/ml in 6 M guanidine-HCl, 50 mM Tris-HCl, pH 8.0, by stirring overnight at 4 °C. The sample was centrifuged at 4 °C at 12,000 rpm (SS-34 rotor) for 20 min to remove any undissolved protein. The resulting protein solution (4 ml) was added to the refolding buffer (50 mM Tris-HCl, pH 8.0, 0.9 M guanidine-HCl, 0.8 M NaCl, 10 mM $CaCl_2$, 5 mM freshly added cysteine, 5 mM lauryl sulfobetaine), and refolding was allowed to proceed as had been performed for human group IIF sPLA$_2$ (19). The protein solution was concentrated to 40–50 ml in a stirred cell with a YM-10 membrane (Amicon) and then dialyzed against 20 mM sodium phosphate, pH 6.6, 5 mM lauryl sulfobetaine, 1 mM methionine at 4 °C. Trypsin was added (0.5 μg/ml), and digestion was allowed to proceed at room temperature for 12–15 h. The enzymatic activity was increased about 30-fold following digestion. Phenylmethylsulfonyl fluoride was added to 0.5 mM, and the solution was stored for several hours at 4 °C or at −20 °C for longer periods.

The trypsin-digested hGX was purified by ion-exchange HPLC on a Tosohaas DEAE-3SW column (0.75 × 15 cm) equilibrated with 20 mM sodium phosphate, pH 6.7, 30% CH_3CN, 1 mM methionine (buffer C). The resulting protein solution (10 ml) was injected onto the HPLC column pre-equilibrated with buffer C and was developed with the following gradient: 0–12% solvent D (solvent C + 1.0 M NaCl) over 30 min, then 12–100% D over 4 min at 3 ml/min. The hGX peak eluted at 25 min. The material was further purified by a 5-ml injection of a hGX solution onto a reverse phase HPLC (Vydac 218TP1010) using solvent E (20% CH_3CN, 0.1% trifluoroacetic acid, 1 mM methionine) and solvent F (100% CH_3CN, 0.1% trifluoroacetic acid, 1 mM methionine) equilibrated with solvent E, then using the following gradient: 0–12.5% F over 2 min, 12.5–20.6% F over 48 min, and 20.6–100% F over 4 min at 3.0 ml/min. The hGX peak eluted at 40–44 min. The HPLC fraction was neutralized by the addition of 10 μl of 2.0 M Tris base per 1 ml of HPLC fraction. The pooled fractions were concentrated to 60–70% of the initial volume on a rotary evaporator, and lauryl sulfobetaine was added to 5 mM. The solution was concentrated to the desired final concentration (2–10 mg/ml) using a Centriprep-10 and finally dialyzed against 20 mM Tris-HCl, pH 8.0, 1 mM methionine. The protein was judged to be >98% pure on a 15% SDS-PAGE gel. The observed M_r (electrospray mass spectrometry) was 13,614.7, compared with a calculated M_r of 13,615.5.

Crystallization and X-ray Data Collection—Protein crystal growth experiments were designed to obtain crystals of the Ca^{2+}-coordinated hGX enzyme with and without the bound competitive inhibitor MJ33. Protein crystal screening of hGX was carried out using the hanging drop method (20) at 25 °C and commercially available matrices (Hampton Research). Hanging drops were made of hGX co-crystallized in the presence of the inhibitor MJ33 by mixing 2.0 μl of a stock solution containing 15 mg/ml protein, 10 mM $CaCl_2$, and 3 mM MJ33 with 2.0 μl of a reservoir solution of 10 mM $CaCl_2$, 12% PEG 3500, 10% 2-methyl-2,4-pentanediol (MPD), 2% ethylene glycol, and 0.2 M Hepes buffer, pH 7.4. Rectangular shaped crystals appeared in 3 days and were allowed to grow for 3 weeks before data collection. Protein crystals were obtained from hGX without the inhibitor MJ33 under identical conditions as those listed above except that the reservoir solution was buffered at pH 7.6. In this case, tetragonal-shaped crystals appeared in 3 days and were allowed to grow for 3 weeks before data collection.

X-ray diffraction data sets were collected for two hGX crystal forms on a Rigaku RU-H3R rotating anode generator with a RAXIS IV image plate area detector. For the hGX crystal form with MJ33 present, two crystals were needed to collect a complete data set. Otherwise, both crystal forms were pretreated in a similar fashion. Each required the introduction of a cryo-protecting and stabilizing solution made of the crystallization condition reported above with the addition of glycerol as the cryo-protectant at a concentration of 10% (w/v), then flash frozen in the −180 °C nitrogen cryostream. The Programs DENZO and SCALEPAK (21) were used for data processing and scaling.

Molecular Replacement—Molecular replacement was performed using the program AMORE (22) to solve the crystal structure of hGX. The structure was first solved for the hGX $P2_1$ crystal form grown in the absence of MJ33. A group IIA sPLA$_2$ structure from Chinese cobra (Protein Data Bank number 1POB) was used as the initial search model (23). The cobra venom protein sequence was 29% identical and 39% similar to the hGX enzyme. Three independent solutions were found in the rotational search with a peak intensity almost twice above the noise level. The translation search gave a unique solution of 3 subunits within the asymmetric unit and with a final correlation factor of 28.1% and *R*-factor of 46.9%. The refined hGX model was then used to solve the structure of the second crystal form ($C222_1$) grown with MJ33 present in the crystallization condition. This crystal form had two subunits of hGX in the asymmetric unit, and the translation search gave a final correlation factor of 59% and an *R*-factor of 38%.

Crystallographic Refinement—Standard refinement procedures using the program CNS (24) were successful in obtaining a reliable model in each crystal form. Iterative model improvement was done using the programs CHAIN (25) and O (26). In refining the structure in space group $P2_1$, the initial model obtained from molecular replacement was subjected to a round of rigid body, positional, individual temperature factor (*B*-factor), and simulated annealing (5000 K) refinement to 2.5 Å, resulting in an R_{free} of 0.474 and an $R_{working}$ of 0.388. At this point, the correct sequence of hGX (gi:4505845) was introduced into the refinement model. After one round of positional and simulated annealing refinement the R_{free} and $R_{working}$ was 0.415 and 0.335, respectively. With 483 solvent molecules built into the model and extending the resolution to 1.97 Å, the final R_{free} was 0.232 and $R_{working}$ was 0.190 with good geometry. Refinement of the $C222_1$ crystal form was more straightforward, starting from the nearly final model from the $P2_1$ crystal form. The model for this crystal form was refined to a resolution of 2.09 Å, and included 248 waters added to the model, yielding an R_{free} and $R_{working}$ of 0.252 and 0.211, respectively, with good geometry.

Catalytic Function and Interfacial Binding of hGX—These measurements were performed at 24 °C and pH 8.0 under conditions specified in the figure legends. Procedures already established for other secreted PLA$_2$ enzymes were used for the characterization of hGX, and the results unique to hGX were developed in detail (4, 5). For example, the initial rate of hydrolysis of DC_7PC was compared by the pH stat (27) and the fluorescent pH indicator dye methods (28). Formation of the premicellar aggregates with 1,2-dihexylglycero-*sn*-3-phosphocholine (DC_6PC-ether) was monitored as a change in the 90° scattering at 360 nm with an SLM-aminco fluorimeter.

RESULTS

Structural features of the 1.97-Å crystal structure of a ligand-free form of hGX are described and interpreted in relation to its functional characteristics. The statistics of the x-ray data collection and refinement of two crystal forms of hGX are summarized in Table I. As expected the protein fold of hGX was quite similar to previously reported sPLA$_2$ structures. The predicted disulfide-bonding pattern (9) that led to the classification of hGX as a group X enzyme has been confirmed to contain 8 disulfide bonds. Beyond predictions of a novel protein fold, other potential structural differences can be predicted by gazing at a sequence alignment of sPLA$_2$ family members, as shown in Fig. 1. The hGX enzyme was between 29 and 41% identical to other members of the 14-kDa family of sPLA$_2$ enzymes. Residues that were part of the active site were highly conserved, and as expected, the active site of the hGX structure was remarkably similar to the previously solved group IB (29) and group IIA (30, 31) enzymes. However, there were noticeable differences in the hGX structure, relative to the group IB and IIA enzymes, and in the i-face binding surface. The asso-

TABLE I
X-ray data collection and refinement of hGX sPLA$_2$ ligand free structures

hGX crystal form	hGX (no MJ33)	hGX (with MJ33)
Crystal data		
Space group	$P2_1$	$C222_1$
Cell parameters		
a (Å)	51.2	139.1
b (Å)	62.1	145.1
c (Å)	70.4	28.1
β (°)	99.3	
Subunits/asymmetric unit	3	2
X-ray data		
Total reflections	337,721	184,444
Unique reflections	34,475	19,931
Resolution limit (Å)	1.90	2.00
Completeness (%)	99.8	95.8
R_{merge} [a] (%)	6.3	8.1
Refinement		
Resolution range (Å)	6.0–1.97	6.0–2.09
$R_{working}$ [b]	0.190	0.252
R_{free} [b]	0.232	0.211
RMSD observed		
Bond length (Å)	0.005	0.005
Angle (°)	1.16	1.14
Total protein atoms	2835	1890
Total water molecules	481	259

[a] $R_{merge} = \Sigma|I_o - I_a|/(I_a)$, where I_o is the observed intensity and I_a is the average intensity, the sums being taken over all symmetry related reflections.

[b] R-factor $= \Sigma|F_o - F_c|/(F_o)$, where F_o is the observed amplitude and F_c is the calculated amplitude. R_{free} is the equivalent of $R_{working}$, except it is calculated for a randomly chosen set of reflections that were omitted (5%) from the refinement process (52).

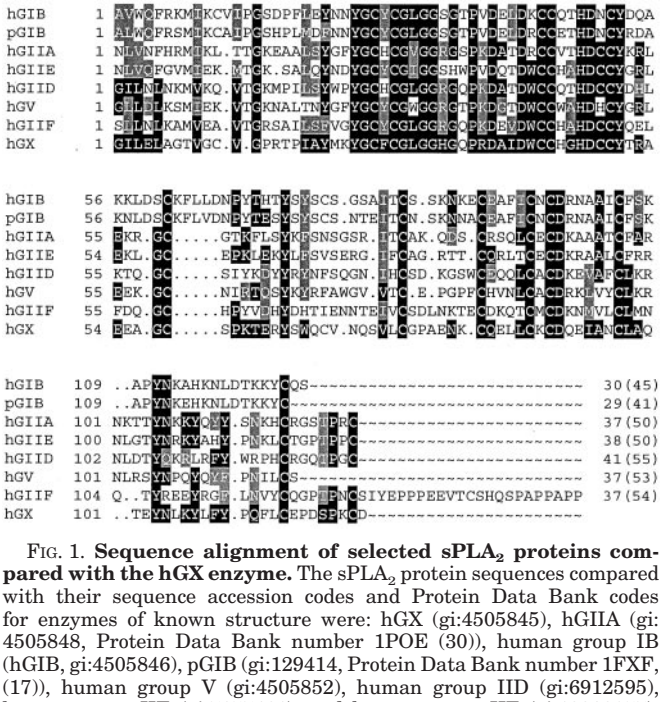

FIG. 1. **Sequence alignment of selected sPLA$_2$ proteins compared with the hGX enzyme.** The sPLA$_2$ protein sequences compared with their sequence accession codes and Protein Data Bank codes for enzymes of known structure were: hGX (gi:4505845), hGIIA (gi:4505848, Protein Data Bank number 1POE (30)), human group IB (hGIB, gi:4505846), pGIB (gi:129414, Protein Data Bank number 1FXF, (17)), human group V (gi:4505852), human group IID (gi:6912595), human group IIE (gi:7657461), and human group IIF (gi:12383057). The other two known human sPLA$_2$ sequences, group III and group XII, were not included because their sequences differ dramatically to the sequences presented here. The percent identity (and similarity) of each sequence relative to hGX is indicated at the end of each sequence. This alignment was performed using PILEUP from the GCG software and displayed with the program BOXSHADE.

ciated active site slot provides significant insights into the functional differences between these paralogs. These structural observations provide a framework to understand the substrate

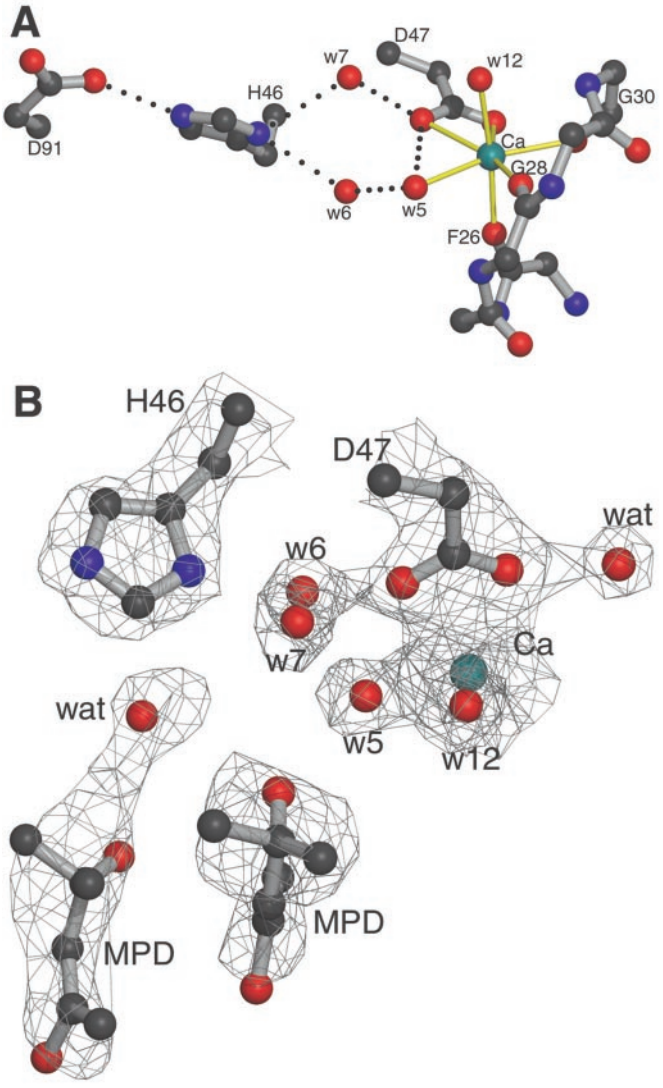

FIG. 2. **Active site and Ca^{2+} coordination in the hGX structure.** *A*, *ball* and *stick model* of hGX from the $P2_1$ crystal form, which was grown without the inhibitor MJ33. The active site is shown including residues Asp-91, His-46, Asp-47, and the catalytic Ca^{2+}. The first and second sphere waters of the Ca^{2+} are likewise shown. The Ca^{2+} coordination includes carbonyl backbone interactions from Phe-26, Gly-28, and Gly-30, waters w5 and w12, and finally a shared bidentate interaction from Asp-47. *B*, electron density difference map (coefficient $2F_o - F_c$) drawn at a 1.0-σ cutoff of the active site of hGX crystal form $C222_1$ grown in the presence of the inhibitor MJ33. The view shown is a *top down view* of *A*. The active site residues, Ca^{2+}, and bound water molecules are nearly identically placed relative to that observed for the hGX $P2_1$ crystal form (*A*), which was grown without MJ33. All of the Ca^{2+}-coordinated waters (first and second shell) are modeled into well defined electron density. Two molecules of the compound MPD were modeled into the active site. The figure was made using the programs MOLSCRIPT (50), POVSCRIPT (E. Peisach and D. Peisach), and POVRAY (www.povray.org).

preference and kinetic differences observed for hGX compared with the group IB and IIA enzymes.

Active Site Coordination of hGX—The active site of the hGX structure for crystals of both crystal forms ($P2_1$ and $C222_1$) are shown in Fig. 2. The ligand-free structure of hGX (Fig. 2*A*) shows an arrangement of side chains, calcium coordination, and bound waters that was virtually identical to the structures of group IB and IIA sPLA$_2$ structures without bound ligands (29, 30). Just as has been observed in the group IB and IIA structures, the catalytic Ca^{2+} has octahedral geometry with 7 coordinating oxygen ligands with Ca^{2+}-oxygen distances that range from 2.3 to 2.6 Å. The Ca^{2+}-binding loop was comprised

of three carbonyl oxygens from Phe-26, Gly-28, and Gly-30. The two carboxylate oxygens of Asp-47 share an equatorial coordination site to Ca^{2+}. The remaining positions were occupied by the axial water w12 and the equatorial water w5, often referred to as the catalytic water. The second sphere waters, w6 and w7, bridge the acid/base catalyst His-46 and the Ca^{2+} ligands w5 and Asp-47. The conservation of an hGX active site including active site residues and mechanistically critical waters suggests a conserved mechanism of this class of sPLA$_2$ enzyme.

hGX Co-crystallized with MJ33 Yielded a Ligand-free Structure—Two crystal forms were obtained of hGX controlled by whether or not the inhibitor MJ33 was added. The crystal form grown in the absence of MJ33 was in the $P2_1$ space group and had 3 subunits of hGX in the asymmetric unit. The crystal form grown with MJ33 at a saturating concentration (3 mM) was in the space group $C222_1$ with 2 subunits in the asymmetric unit. However, this crystal form also yielded a ligand-free crystal structure. The active site of the hGX structure from crystals that were grown in the presence of MJ33 is shown in Fig. 2*B*. The electron density map ($2F_o - F_c$) unequivocally identifies this as a ligand-free structure. Careful examination of $F_o - F_c$ difference electron density maps confirmed the absence of a substrate-mimic ligand bound to the Ca^{2+}. Difference density was located farther from the bound Ca^{2+}, which led to the modeling of two molecules of MPD into the hGX active site (Fig. 2*B*). The position of these MPD molecules was very similar to the placement of MPD solvent molecules into the 0.97-Å crystal structure of bovine group IB sPLA$_2$, which was likewise ligand free (29).

Comparison of hGX to Group IB and IIA sPLA$_2$ Structures—As one would expect from the alignment of sPLA$_2$ sequences (Fig. 1), the main chain C_α-trace of hGX resembles the group IIA structures more than the group IB pancreatic enzymes. An overlay of group X, IIA, and IB enzymes was shown in Fig. 3 highlighting some minor, yet potentially significant differences. The group IB enzymes have an insertion of 5 residues (amino acids 62–66, Fig. 1) relative to the hGX and human group IIA (*hGIIA*) sequences. The overlay shown in Fig. 3*A* demonstrates the result of this difference by a significantly altered surface loop (amino acids 59–75) for the porcine group IB enzyme (*pGIB*) shown at the top of the figure. Tyr-69 of group IB enzymes binds with the *sn-3* phosphate moiety of the substrate mimics (32–34). The analogous position in the group X and IIA enzymes contains a lysine residue at this position, which likewise interacts with the *sn-3* phosphate moiety of an inhibitor complex with the hGIIA enzyme (30). It was also significant that the differences of this i-face surface loop greatly affect the size and shape of the sPLA$_2$ active site. The other notable difference was the C-terminal extension of group X and IIA structures relative to the group IB structures.

More subtle differences exist between hGX and the group IIA C_α traces shown in Fig. 3*B*. For example, the hGX structure has a slightly modified position of the surface loop from amino acid position 14 to 20 (14–20 loop) of the hGX sequence. This loop is labeled in the *bottom* of Fig. 3*B*, and was likely critical for i-face binding. This loop begins with a proline residue at position 14, which varies in many of the other sPLA$_2$ family members (Fig. 1). It is noteworthy that this proline exists in both a *cis*-proline and *trans*-proline form in the hGX structures reported here. Remarkably, subunit A of the $C222_1$ crystal form has a *cis*-proline at position 14, whereas subunit B from the same structure has a *trans*-proline at the same position. In contrast, all three prolines at position 14 of the $P2_1$ crystal form exist in the *trans* form. Pro-78 of the hGX structure was modeled as a *cis*-proline in 4 of the 5 independent views of the hGX structure; one of the subunits of the $P2_1$ crystal form had one of the Pro-78 residues modeled in the *trans*-conformation. In each case, the *cis*-prolines at positions 14 or 78 made crystal contacts with other subunits of the crystal structures. Likewise, the *trans*-proline forms at positions 14 and 78 were observed when no such crystal contacts existed. Despite these subtle C_α trace differences, the group X and IIA enzymes show considerable homology. In the absence of an active site directed ligand bound to hGX, the structure of the hGIIA enzyme complexed with the inhibitor 1-*O*-octyl-2-heptylphosphonyl-*sn*-glycero-3-phosphoethanolamine (Fig. 3, Protein Data Bank number 1POE) serves

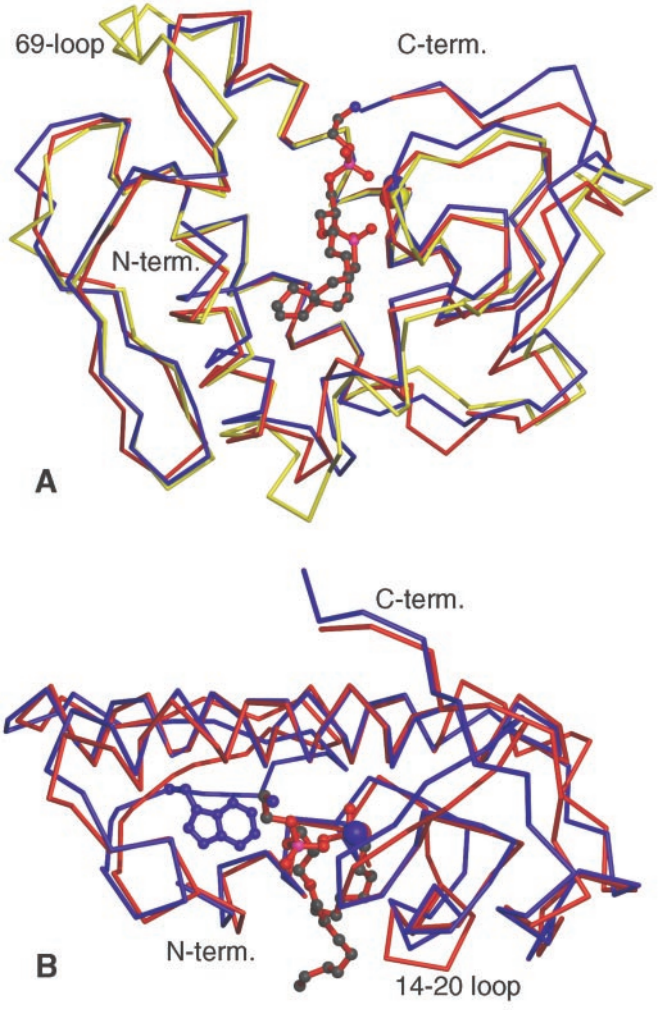

FIG. 3. **Comparison of hGX to other sPLA$_2$ family members.** *A*, C_α trace comparison of hGX subunit A (*blue*) with two sPLA$_2$ structures: hGIIA with the tetrahedral transition state analog 1-*O*-octyl-2-heptylphosphonyl-*sn*-glycero-3-phosphoethanolamine bound (*red*, Protein Data Bank number 1POE (30)) and pGIB (*yellow*, Protein Data Bank number 1FXF (17)). The plane of the i-face-binding region of hGX is shown to the *front* of this view, with the active site pocket in the center of the structure. The position of the i-face surface loop from amino acids 59 to 75 of the pGIB structure is labeled as the 69-loop because of the importance of Tyr-69. *B*, comparison of hGX (*blue*) with the hGIIA sPLA$_2$ (*red*) with the tetrahedral transition state analog 1-*O*-octyl-2-heptylphosphonyl-*sn*-glycero-3-phosphoethanolamine bound (Protein Data Bank number 1POE (30)). The catalytic Ca^{2+} ions of the hGX and hGIIA structures are likewise shown in *red* and *blue*, respectively. The i-face of the sPLA$_2$ structures is *facing the bottom* of the figure with the alkyl chain of the inhibitor pointing down. Also shown is the interfacial residue Trp-67 from the hGX structure (*blue*). The i-face surface loop from amino acids 14 to 20 of the hGX structure is labeled. The structures were aligned over their two long α-helices (amino acids 42–53, 86–99 in hGX; amino acids 43–54 and 86–99 in hGIIA; amino acids 44–55 and 94–107 in pGIB). The figure was made using the programs MOLSCRIPT (50), POVSCRIPT (E. Peisach and D. Peisach), and POVRAY (www.povray.org).

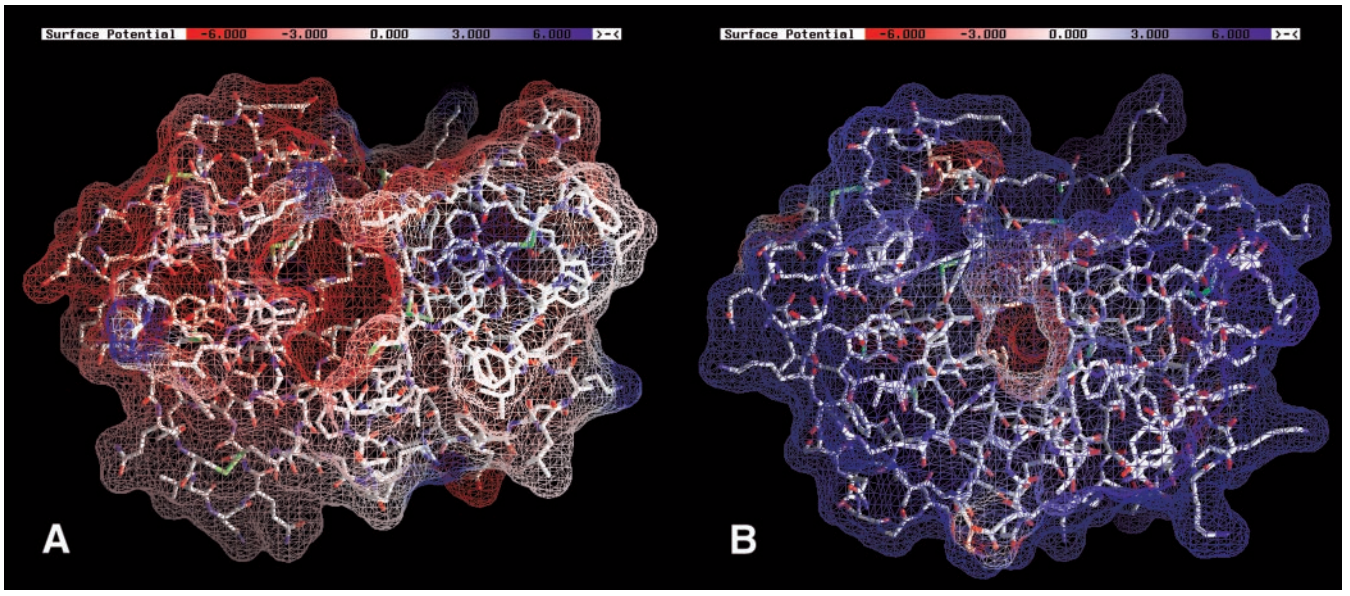

FIG. 4. **Electrostatic surface potentials of hGX (*A*) and hGIIA (*B*) in a ligand-free form (Protein Data Bank number 1POD (30)).** The view shown for each structure presents the i-face binding surface of the enzyme. The active sites shown in the center of each structure have noticeably different sizes and shapes. The sPLA$_2$ model of each structure is displayed in *stick format* with CPK colors. The potential surface is displayed color-coded onto a meshed van der Waals surface using the program GRASP (51), where *red* and *blue* represent a net negative and positive charge and *white* represents overall neutral positions, respectively.

as a useful model to predict potential differences in substrate and inhibitor specificity (30). Although C_α overlays demonstrate a very similar core structure, considerable differences exist on the i-face surface of these two enzymes, as well as the entrance of their active site pockets.

Electrostatic Potential and van der Waals Surface of hGX—The critical functional features of sPLA$_2$ are intricately controlled by how the enzyme interacts with its substrate interface. Experimental approaches have led to a prediction of not only which surface of the sPLA$_2$ enzymes interact with the interface, but additionally the specific nature of these interactions (5, 16, 17, 35). An electrostatic potential and van der Waals surface comparison of the i-face of hGX *versus* hGIIA is displayed in Fig. 4, which shows the most dramatic, and likely, the most significant differences between these two enzymes. The human synovial fluid group IIA enzyme displays an extensively positive charged i-face surface. In contrast the hGX i-face surface was mainly nonpolar in nature and therefore electrostatically neutral. Another striking difference can be observed (Fig. 4) from a comparison of the van der Waals surface of the active site opening of ligand-free structures of hGX *versus* hGIIA. The hGX active site was considerably more open, possibly indicating a functional need to accommodate substrates with polyunsaturated *sn-2* chains, such as arachidonate. Among mammalian sPLA$_2$s, hGX and mouse group X display the largest preference for phospholipid with an *sn-2* arachidonyl chain *versus* a palmitoyl chain based on relative interfacial k_{cat}/K_m values.[2] For example, the hGIIA enzyme with a considerably narrower active site opening on the i-face (Fig. 4) is 3-fold less specific than hGX for an arachidonyl *versus* palmitoyl chain at the *sn-2* position.

High Activity of hGX on Zwitterionic Interfaces—In light of the different i-face of hGX in comparison to that of hGIIA (Fig. 4), it was of interest to explore the kinetic behavior of hGX acting on zwitterionic interfaces. The apparent parameters for the kinetic characterization of hGX on the various forms of substrates are summarized in Table II. The hGX initial rate (v_o) of hydrolysis at $X_S = 1$ on dimyristoyl-*sn*-3-phosphomethanol vesicles was only 10 s^{-1} compared with 270 s^{-1} for the pGIB (36) and 90 s^{-1} for hGIIA (37). Although the reaction progress in the scooting mode was not observed with hGX on zwitterionic DMPC vesicles, a high affinity for the zwitterionic interface was indicated by the kinetic parameters (see below) underlying a comparatively high activity of 20 s^{-1} for hGX compared with initial v_o values that were close to zero for the hydrolysis of DMPC vesicles by pGIB and hGIIA sPLA$_2$s (38–40). In short, the most significant difference between the hGX relative to pGIB and hGIIA was in a dramatically higher ability of hGX to hydrolyze substrates at a zwitterionic interface.

TABLE II
Kinetic parameters for hGX sPLA$_2$

Substrate	v_o	V_{max}^{app}[a]	K_M^{app}
		(s^{-1})	(mM)
DMPM vesicles[b]	10		
Dithio-DMPM vesicles[b]	9		
DMPC vesicles[b]	20		
DC_7PC monomer		20	0.25
DC_7PC micelle in 1 mM NaCl		45	0.43
DC_7PC micelle in 4 M NaCl		34	0.12

[a] The apparent rate parameters were obtained by fitting the concentration dependence of the observed initial rate under the respective conditions (41). Thus V_{max}^{app} is the initial rate at $X_s = 1$, and K_m^{app} is the affinity of the enzyme for the micellar interface. The fit parameters V_{max}^{app} and K_m^{app} have estimated errors of 30% or their reported values.
[b] v_o is the observed initial rate for substrates at a mole fraction $X_S = 1$. Initial rates were reproducible to within an error range of 10% of each value.

The behavior of hGX on the micellar interface of zwitterionic DC_7PC has been characterized in detail here because it differs significantly from that of pGIB and hGIIA sPLA2s. The initial rate of hydrolysis by hGX of DC_7PC at several concentrations is shown in Fig. 5, and the kinetic constants, K_m^{app} and V_{max}^{app} (41), were extracted from these results and are listed in Table II. These rates, under the stirred or unstirred conditions, were measured by monitoring the fluorescence of a pH indicator dye (28). Comparable results were also obtained in the pH stat assay, which can be carried out only with a stirred reaction mixture. This assay includes contributions from the reaction in solution as well as the extraneous surfaces of the vessel walls

[2] M. H. Gelb, unpublished data.

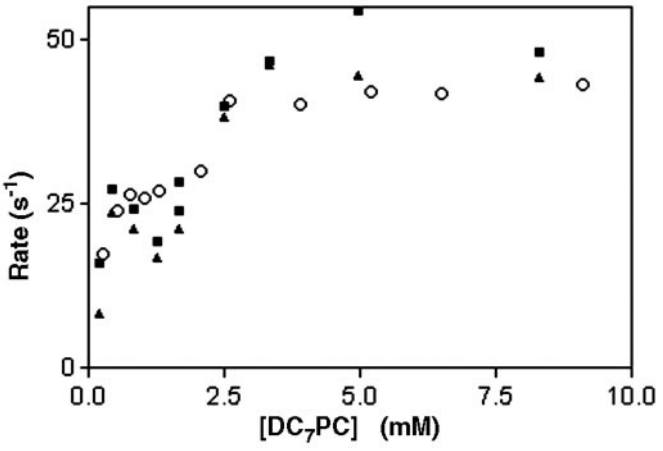

FIG. 5. **The concentration dependence of the initial rate of hydrolysis of DC_7PC (CMC of 1.5 mM).** The rate of hydrolysis was measured as a change in the fluorescence from a pH-indicator dye (28) for the rate in an unstirred solution (*solid triangles*), the rate in a stirred solution (*filled squares*), and rates measured by the pH stat (27) (*open circles*) method in a vigorously stirred solution.

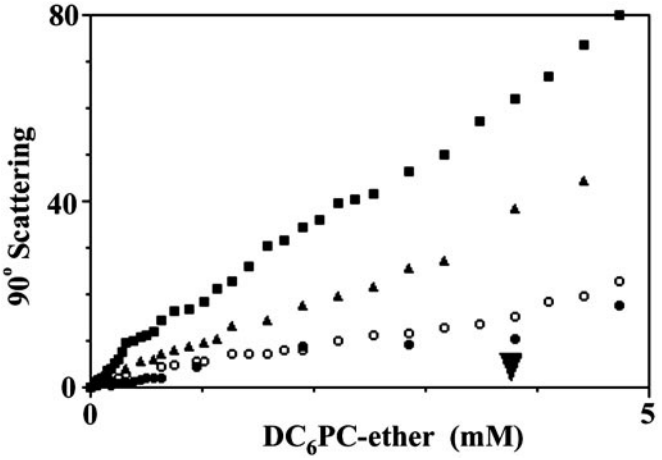

FIG. 6. **The change in the 90° scattered light at 360 nm as a function of added DC_6PC-ether.** The CMC of 3.9 mM is marked on the *x* axis. The conditions compared are: no enzyme with 10 mM Tris, 5 mM $CaCl_2$ at pH 8.0 and 24 °C (*closed circles*), with pig pancreatic IB PLA2 in 5 mM $CaCl_2$, where the points track slightly above the controls with no protein added (*open circles*), with 2 μM hGX, 1 mM EGTA, and 1 mM EDTA (*triangles*), and with 2 μM hGX and 5 mM $CaCl_2$ (*squares*). Controls showed that Ca^{2+} has no detectable effect on the scattering of hGX.

and air bubbles (27). The maximum rate of hydrolysis below the critical micelle concentration (CMC) of DC_7PC was about 25 s^{-1} compared with the rate of 45 s^{-1} at the saturating concentration of DC_7PC (Fig. 5). Note that $V_{max}{}^{app}$ remains virtually the same in the presence of 4 M NaCl even though $K_m{}^{app}$ decreases by a factor of three. The decrease in $K_m{}^{app}$ was most likely because of the salt-induced hydrophobic effect, which increases the affinity of the enzyme for the interface and also lowers the CMC of the micellar substrate (41). On the other hand, when comparing rates with 1 mM *versus* 4 M NaCl added, there was only a marginal change in the value of $V_{max}{}^{app}$. At high concentrations of NaCl the phosphatidylcholine interface becomes negatively charged because of a preferential partitioning of chloride anions (42). This increase in negative charge does not appear to affect the hGX chemical step. This was consistent with kinetic data with phospholipid vesicles (Table II) showing that the rate of hydrolysis by hGX was not influenced significantly by the anionic charge at the interface.

Several features of these results are noteworthy especially in relation to the behavior seen with pGIB (41). The rate of hydrolysis below the CMC of DC_7PC was significant: 20 s^{-1} with hGX compared with <0.03 s^{-1} with pGIB. Similarly, as summarized in Table II the rate enhancement above the CMC is only 2-fold for hGX, and the rate of hydrolysis of the micellar DC_7PC does not change in the presence of 4 M NaCl. In contrast, with pGIB the rate above the CMC was 15 s^{-1}, and a further 50-fold rate enhancement was seen in the presence of 4 M NaCl.

The origin of a significant rate of hydrolysis of monodisperse DC_7PC by hGX was examined further. A small difference between the rates in the stirred and unstirred solution (Fig. 5) suggests that the contribution of the rates from the reaction on the walls of the reaction vessel was small compared with the rate of hydrolysis of the monodisperse substrate. This was consistent with the possibility of the formation of a monodisperse hGX-DC_7PC complex in aqueous solution. However, it was also possible that hGX forms premicellar aggregates with monodisperse substrate in which the turnover occurs via an interfacial form of the Michaelis complex E^*S. In fact, results summarized in Fig. 6 show that premicellar aggregates were formed between hGX and the nonhydrolyzable DC_6PC-ether amphiphile. The DC_6PC-ether in the absence of enzyme remains monodisperse up to 4 mM. The increase in the intensity of the scattered light in the presence of hGX and monodisperse

TABLE III
Inhibition of hGX sPLA$_2$ DMPM hydrolysis

Inhibitor[a]	X_I50[b]
MJ33	0.052
MJ50	0.03
Oleoylamide (*cis*)	0.011
Elaidoylamide (*trans*)	0.0055
Masticadienoic acid	0.055
HK40	0.022
PG-utrecht	0.0058
PC-utrecht	0.0017
Zn^{2+}	2.5 μM
MPD	300 mM

[a] MJ50, 1-hexadecyl-3-(trichloroethyl)-*sn*-glycero-2-phosphomethanol; HK40, 1-deoxy-1-octylthio-2-heptylphosphonyl-*sn*-glycero-3-phosphoethanol; masticadienoic acid (53); PC-utrecht, (*R*)-2-*O*-decanoylamino-octanol-1-*O*-phosphocholine; PG-utrecht, (*R*)-2-*O*-decanoylamino-octanol-1-*O*-phosphoglycol; PC-utrecht and PG-utrecht were kindly provided by Professor de Haas (Utrecht).

[b] The inhibitor concentrations that produce half-activity of DMPM hydrolysis, IC_{50}, are reported in micromolar for Zn^{2+} and MPD. For the other inhibitors, which are assumed to be completely partitioned in the DMPM interface, X_I50 is the mole fraction of the inhibitor that gives half-activity (18). The reported values of X_I50 are reproducible to within 10% of each value.

DC_6PC-ether indicates the formation of premicellar aggregates. Moreover, the scattering increase was larger in the presence of calcium than without calcium added. The initial E to E^* step does not require Ca^{2+}. However, $sPLA_2$ enzymes require a bound Ca^{2+} to bind substrates or substrate mimics. Therefore, according to the detailed balance condition (5, 41), the apparent tendency to form a premicellar aggregate would increase in the presence of Ca^{2+}. The observed formation of such premicellar aggregates makes it quite likely that the hGX catalyzed hydrolysis of substrates proceeds at the interface via an interfacially active E^*S form of the enzyme even though the bulk of the substrate amphiphile remains monodisperse in the reaction mixture. Under this scenario, the reaction progress can proceed at a rapid rate at such an interface, so long as the rate of substrate replenishment is rapid (5, 41).

DISCUSSION

As is apparent from other $sPLA_2$ structures, the hGX structure reaffirms a clear dissection of the active site and the i-face.

Operationally, the difference is useful for assigning independent roles for the structural features involved in the events of the catalytic cycle and the binding of the enzyme to the interface. Results at hand show that while retaining the architecture of the catalytic site, the i-face of hGX was significantly different from several other sPLA$_2$s. The hGX PLA$_2$ has the ability to form premicellar aggregates with zwitterionic amphiphiles, and it hydrolyzes zwitterionic and anionic phospholipid vesicles with similar catalytic efficiency (Table II). In these respects, hGX behaves like cobra venom sPLA$_2$ (39, 43) and is the first mammalian sPLA$_2$ shown to have these properties. The rate of hydrolysis of DC$_7$PC by hGX (Fig. 5) and cobra venom sPLA$_2$ (39, 43) shows only a modest increase when the substrate concentration is increased above its CMC. This initially gives an impression that these enzymes do not exhibit the classical interfacial activation that is the hallmark of other sPLA$_2$s such as pGIB (3). However, the lack of a large increase in rate above the CMC value of DC$_7$PC is presumably because, well below the CMC value of the substrate, hGX forms its own interface as a protein-lipid premicellar aggregate (Fig. 6). The structure of the hGX enzyme has a more pronounced hydrophobic patch than the group IB and IIA enzyme. This surface is likely critical for premicellar interaction with the hydrophobic tails of the DC$_7$PC substrate. Additionally, the dramatically different electrostatic potentials of the hGIIA and hGX i-faces (Fig. 4) provide a working hypothesis for the structural basis for the observed interfacial binding selectivity with preformed interface (Table II) as well as for the formation of premicellar aggregates. These structural differences observed between the hGX and hGIIA i-face residues likewise set the stage for an investigation of their functional differences by detailed site-directed mutagenesis studies.

The effects of the interface and the anionic charge on the catalytic efficiency of hGX *versus* pGIB and hGIIA were dramatically different. Under optimal conditions with optimal substrate interface to bind all the enzyme, the turnover rate at the maximum substrate mole fraction $X_s^* = 1$ is about 20-fold higher for pGIB (36, 41), and is 4-fold higher for hGIIA (37) than that for hGX. At this stage we cannot ascertain if the lower rate with hGX was because of a higher K_m^* or an impaired k_{cat}^*. However, it was of interest to note that the affinity of hGX for the various inhibitors (Table III) was of comparable magnitude to that for other sPLA$_2$s. If K_m^* for the substrate was controlled through the same interactions as the binding of inhibitors, the change in the rate at $X_S = 1$ would suggest an impaired k_{cat}^* for hGX. A compromised chemical step is also indicated by the observation that the hGX enzyme does not kinetically distinguish between the oxy- or thio-dimyristoyl-*sn*-3-phosphomethanol (Table II). This contrasts with the reported dimyristoyl-*sn*-3-phosphomethanol oxy/thio ratio of about 12 for pGIB, which is thought to have a rate-limiting chemical step (44).

The lack of the inhibitor MJ33 in the hGX C222$_1$ crystal form was initially disconcerting. However, a simple explanation is that the active site of hGX has been out competed by the MPD solvent molecules instead of the MJ33 inhibitor. Further attempts are in progress to obtain structures of the hGX enzyme with bound active site ligands. In the absence of such structures, structure alignments with other inhibitor-bound sPLA$_2$ structures can be used to predict potential differences. Specifically, this comparison has been done between the hGX from this work and the hGIIA bound to a tetrahedral mimic inhibitor (30) enzymes as shown in Fig. 3*B*. Although the structure of the active site of sPLA$_2$s is highly conserved, the residues that line the active site slot are not identical among these enzymes. Thus, it has been possible to discover active site inhibitors that display significant selectivity among various sPLA$_2$s. For example, MJ33 is a potent inhibitor of pGIB (18) but is not an inhibitor of human group IIA sPLA$_2$ (37). Likewise, the indole-3-acetamide analog LY311727 (45) and related analogs (46, 47) bind about 2 orders of magnitude tighter to hGIIA and human group IIE sPLA$_2$ than to hGX and human group V sPLA$_2$. Because the x-ray structures of three of these indole-3-acetamide analogs bound to hGIIA have been determined (48), the variation in the active site residues that contact the inhibitor among the different mammalian sPLA$_2$s can be compared. Most of these residues are invariant among the different enzymes, but two notable exceptions are seen. Leu-5 and Leu-98 of hGX are conserved in human group V sPLA$_2$ but are replaced by phenylalanines in the hGIIA and human group IIE sPLA$_2$. In the hGIIA structure, Phe-5 and Phe-98 are well packed against the face of the indole ring of the bound inhibitor. Substitution by leucine in hGX and human group V sPLA$_2$ would be expected to leave a gap between the enzyme and inhibitor that would not be ideal for high affinity binding. The x-ray structure of hGX reported here is expected to facilitate the development of potent and selective inhibitors of hGX.

To understand the determinants of potent inhibitors and substrate specificity there are additional issues to consider beyond a comparison of active site residues and the charged nature of the i-face of the enzymes. In general, sPLA$_2$ enzymes have been suggested to undergo structural changes upon binding an interface (4). It is speculated that many of these changes are mediated by surface loops that are part of the i-face of the enzyme. The observation of both *cis*- and *trans*-proline at position 14 of hGX may be of significance to determining interfacial activity and/or specificity. The *cis*/*trans* observation suggests that the proline peptide bond is at equilibrium between the *cis*- and *trans*-conformation. The thermodynamics and rates of *cis*-/*trans*-proline isomerization have been thoroughly studied for nonenzymatic and enzymatic reactions (49). Even on the interface, the rates of isomerization are likely significantly slower than the time scale of the reaction. However, for enzymes like the hGX PLA$_2$ it may be that only one form may be uniquely stabilized in a productive interface bound mode.

REFERENCES

1. Valentin, E., and Lambeau, G. (2000) *Biochim. Biophys. Acta* **1488,** 59–70
2. Six, D. A., and Dennis, E. A. (2000) *Biochim. Biophys. Acta* **1488,** 1–19
3. Verheij, H. M., Slotboom, A. J., and de Haas, G. H. (1981) *Rev. Physiol. Biochem. Pharmacol.* **91,** 91–203
4. Berg, O. G., and Jain, M. K. (2002) *Interfacial Enzyme Kinetics*, Wiley, London
5. Berg, O. G., Gelb, M. H., Tsai, M. D., and Jain, M. K. (2001) *Chem. Rev.* **101,** 2613–2653
6. Murakami, M., Nakatani, Y., Atsumi, G., Inoue, K., and Kudo, I. (1997) *Crit. Rev. Immunol.* **17**, 225–283
7. Kudo, I., Murakami, M., Hara, S., and Inoue, K. (1993) *Biochim. Biophys. Acta* **1170,** 217–231
8. Balsinde, J., Balboa, M. A., Insel, P. A., and Dennis, E. A. (1999) *Annu. Rev. Pharmacol. Toxicol.* **39,** 175–189
9. Cupillard, L., Koumanov, K., Mattei, M. G., Lazdunski, M., and Lambeau, G. (1997) *J. Biol. Chem.* **272,** 15745–15752
10. Jain, M. K., Ranadive, G., Yu, B. Z., and Verheij, H. M. (1991) *Biochemistry* **30,** 7330–7340
11. Bezzine, S., Koduri, R. S., Valentin, E., Murakami, M., Kudo, I., Ghomashchi, F., Sadilek, M., Lambeau, G., and Gelb, M. H. (2000) *J. Biol. Chem.* **275,** 3179–3191
12. Hanasaki, K., Ono, T., Saiga, A., Morioka, Y., Ikeda, M., Kawamoto, K., Higashino, K., Nakano, K., Yamada, K., Ishizaki, J., and Arita, H. (1999) *J. Biol. Chem.* **274,** 34203–34211
13. Morioka, Y., Saiga, A., Yokota, Y., Suzuki, N., Ikeda, M., Ono, T., Nakano, K., Fujii, N., Ishizaki, J., Arita, H., and Hanasaki, K. (2000) *Arch. Biochem. Biophys* **381,** 31–42
14. Morioka, Y., Ikeda, M., Saiga, A., Fujii, N., Ishimoto, Y., Arita, H., and Hanasaki, K. (2000) *FEBS Lett.* **487,** 262–266
15. Scott, D. L., White, S. P., Otwinowski, Z., Yuan, W., Gelb, M. H., and Sigler, P. B. (1990) *Science* **250,** 1541–1546
16. Ramirez, F., and Jain, M. K. (1991) *Proteins Struct. Funct. Genet.* **9,** 229–239
17. Pan, Y. H., Epstein, T. M., Jain, M. K., and Bahnson, B. J. (2001) *Biochemistry* **40,** 609–617
18. Jain, M. K., Tao, W. J., Rogers, J., Arenson, C., Eibl, H., and Yu, B. Z. (1991) *Biochemistry* **30,** 10256–10268
19. Valentin, E., Singer, A. G., Ghomashchi, F., Lazdunski, M., Gelb, M. H., and

Lambeau, G. (2000) *Biochem. Biophys. Res. Commun.* **279,** 223–228
20. Jancarik, J., and Kim, S. H. (1991) *J. Appl. Crystallogr.* **24,** 409–411
21. Otwinowski, Z., and Minor, W. (1997) *Methods Enzymol.* **276,** 307–326
22. CCP4 (1994) *Acta Crystallogr. Sect. D* **50,** 760–763
23. White, S. P., Scott, D. L., Otwinowski, Z., Gelb, M. H., and Sigler, P. B. (1990) *Science* **250,** 1560–1563
24. Brunger, A. T., Adams, P. D., Clore, G. M., Delano, W. L., Gros, P., Grosse-Kunstleve, R. W., Jiang, J.-S., Kuszewski, J., Nilges, N., Pannu, N. S., Read, R. J., Rice, L. M., Simonson, T., and Warren, G. L. (1998) *Acta Crystallogr. Sect. D* **54,** 905–921
25. Sack, J. S., and Quiocho, F. A. (1997) *Methods Enzymol.* **277,** 158–173
26. Jones, T. A., Zou, J. Y., Cowan, S. W., and Kjeldgaard, M. (1991) *Acta Crystallogr. Sect. A* **47,** 110–119
27. Rogers, J., Yu, B. Z., Serves, S. V., Tsivgoulis, G. M., Sotiropoulos, D. N., Ioannou, P. V., and Jain, M. K. (1996) *Biochemistry* **35,** 9375–9384
28. Yu, B. Z., Berg, O. G., and Jain, M. K. (1999) *Biochemistry* **38,** 10449–10456
29. Steiner, R. A., Rozeboom, H. J., de Vries, A., Kalk, K. H., Murshudov, G. N., Wilson, K. S., and Dijkstra, B. W. (2001) *Acta Crystallogr. Sect. D* **57,** 516–526
30. Scott, D. L., White, S. P., Browning, J. L., Rosa, J. J., Gelb, M. H., and Sigler, P. B. (1991) *Science* **254,** 1007–1010
31. Wery, J. P., Schevitz, R. W., Clawson, D. K., Bobbitt, J. L., Dow, E. R., Gamboa, G., Goodson, T., Jr., Hermann, R. B., Kramer, R. M., McClure, D. B., Mihelich, E. D., Putnam, J. E., Sharp, J. D., Stark, D. H., Teater, C., Warrick, M. W., and Jones, N. D. (1991) *Nature* **352,** 79–82
32. Scott, D. L., Otwinowski, Z., Gelb, M. H., and Sigler, P. B. (1990) *Science* **250,** 1563–1566
33. Scott, D. L., and Sigler, P. B. (1994) *Adv. Protein Chem.* **45,** 53–88
34. Thunnissen, M. M., Ab, E., Kalk, K. H., Drenth, J., Dijkstra, B. W., Kuipers, O. P., Dijkman, R., de Haas, G. H., and Verheij, H. M. (1990) *Nature* **347,** 689–691
35. Lin, Y., Nielsen, R., Murray, D., Hubbell, W. L., Mailer, C., Robinson, B. H., and Gelb, M. H. (1998) *Science* **279,** 1925–1929
36. Berg, O. G., Yu, B. Z., Rogers, J., and Jain, M. K. (1991) *Biochemistry* **30,** 7283–7297
37. Bayburt, T., Yu, B. Z., Lin, H. K., Browning, J., Jain, M. K., and Gelb, M. H. (1993) *Biochemistry* **32,** 573–582
38. Apitz-Castro, R., Jain, M. K., and de Haas, G. H. (1982) *Biochim. Biophys. Acta* **688,** 349–356
39. Jain, M. K., Egmond, M. R., Verheij, H. M., Apitz-Castro, R., Dijkman, R., and de Haas, G. H. (1982) *Biochim. Biophys. Acta* **688,** 341–348
40. Jain, M. K., Gelb, M. H., Rogers, J., and Berg, O. G. (1995) *Methods Enzymol.* **249,** 567–614
41. Berg, O. G., Rogers, J., Yu, B. Z., Yao, J., Romsted, L. S., and Jain, M. K. (1997) *Biochemistry* **36,** 14512–14530
42. Yu, B. Z., Poi, M. J., Ramagopal, U. A., Jain, R., Ramakumar, S., Berg, O. G., Tsai, M. D., Sekar, K., and Jain, M. K. (2000) *Biochemistry* **39,** 12312–12323
43. van Eijk, J. H., Verheij, H. M., Dijkman, R., and de Haas, G. H. (1983) *Eur. J. Biochem.* **132,** 183–188
44. Jain, M. K., Yu, B. Z., Rogers, J., Gelb, M. H., Tsai, M. D., Hendrickson, E. K., and Hendrickson, H. S. (1992) *Biochemistry* **31,** 7841–7847
45. Schevitz, R. W., Bach, N. J., Carlson, D. G., Chirgadze, N. Y., Clawson, D. K., Dillard, R. D., Draheim, S. E., Hartley, L. W., Jones, N. D., Mihelich, E. D., Olkowski, J. L., Snyder, D. W., Sommers, C., and Wery, J.-P. (1995) *Nat. Struct. Biol.* **2,** 458–465
46. Suzuki, N., Ishizaki, J., Yokota, Y., Higashino, K., Ono, T., Ikeda, M., Fujii, N., Kawamoto, K., and Hanasaki, K. (2000) *J. Biol. Chem.* **275,** 5785–5793
47. Degousee, N., Ghomashchi, F., Stefanski, E., Singer, A., Smart, B. P., Borregaard, N., Reithmeier, R., Lindsay, T. F., Lichtenberger, C., Reinisch, W., Lambeau, G., Arm, J., Tischfield, J., Gelb, M. H., and Rubin, B. B. (2002) *J. Biol. Chem.* **277,** 5061–5073
48. Mihelich, E. D., and Schevitz, R. W. (1999) *Biochim. Biophys. Acta* **1441,** 223–228
49. Stein, R. L. (1993) *Adv. Protein Chem.* **44,** 1–24
50. Kraulis, P. J. (1991) *J. Appl. Crystallogr.* **24,** 946–950
51. Honig, B., and Nicholls, A. (1995) *Science* **268,** 1144–1149
52. Brunger, A. T. (1992) *Nature* **355,** 472–474
53. Jain, M. K., Yu, B. Z., Rogers, J. M., Smith, A. E., Boger, E. T., Ostrander, R. L., and Rheingold, A. L. (1995) *Phytochemistry* **39,** 537–547